Research Square

Preprints are preliminary reports that have not undergone peer review.
They should not be considered conclusive, used to inform clinical practice,
or referenced by the media as validated information.

Dynamic Flood Routing in Sediment-Affected Reservoirs Using Satellite- Derived Area-Elevation Curves: A Case Study of Golestan Dam, Iran

Abdolreza Zahiri

azahiri@gau.ac.ir

Gorgan University of Agricultural Sciences and Natural Resources

Mohammad Reza Nikoo

Sultan Qaboos University

Hamed Feiz Abady

Gorgan University of Agricultural Sciences and Natural Resources

Article

Keywords: Flood routing, Reservoir sedimentation, Reservoir morphology, Sentinel-2, Google Earth Engine, Golestan Dam Reservoir

Posted Date: September 4th, 2026

DOI: https://doi.org/10.21203/rs.3.rs-10533736/v1

License: This work is licensed under a Creative Commons Attribution 4.0 International License.
Read Full License

Additional Declarations: No competing interests reported.

Dynamic Flood Routing in Sediment-Affected Reservoirs Using Satellite-Derived Area-Elevation Curves: A Case Study of Golestan Dam, Iran

Abdolreza Zahiri [1*] | Mohammad Reza Nikoo[2*] | Hamed Feiz Abady[3]

[1]Associate Professor, Water Engineering Department, Gorgan University of Agricultural Sciences and Natural Resources, Gorgan, Iran, azahiri@gau.ac.ir

[2]Associate Professor, Department of Civil and Architectural Engineering, Sultan Qaboos University, Muscat, Oman, m.reza@squ.edu.om

[3]PhD Student, Water Engineering Department, Gorgan University of Agricultural Sciences and Natural Resources, Gorgan, Iran, Hamedfz1370@gmail.com

[*]Corresponding authors: azahiri@gau.ac.ir; m.reza@squ.edu.om

Abstract: Flood routing is a key component of dam safety evaluation and flood-risk management. Most conventional routing studies assume that reservoir geometry remains constant throughout the service life of a dam and consequently employ the original or design area–elevation curve (AEC). In practice, however, continuous sediment deposition gradually changes reservoir morphology, reduces available storage, and alters the reservoir's hydraulic behavior during flood events. Ignoring these changes may introduce considerable uncertainty into flood-routing analyses and associated risk assessments. This study examines the effects of temporal changes in reservoir geometry on flood-routing results and assesses the potential of satellite remote sensing for updating reservoir geometric characteristics. The Golestan Dam Reservoir in northern Iran was selected as the study area. More than 100 Sentinel-2 images acquired between 2015 and 2025 were processed in Google Earth Engine (GEE) to derive reservoir water surface areas at different water levels using the Normalized Difference Water Index (NDWI). The satellite-derived AEC in 2015 was compared with hydrographic survey results for the same year. This comparison indicated that differences between the two datasets varied with water level and became most pronounced near the spillway crest elevation as well as lower operating levels. The analysis identified substantial morphological changes within the reservoir. The reservoir storage capacity at the spillway crest elevation declined from approximately 86.5 million m³ in 1999 to 51 million m³ in 2015, representing a storage loss of nearly 40%, while sediment accumulation raised the reservoir bed level (thalweg) from about 50.0 m to 55.5 m. The updated AECs were subsequently incorporated into a flood-routing model based on the Modified Puls method and solved using a fourth-order Runge–Kutta numerical algorithm. Flood routing was performed for four design flood hydrographs with return periods of 25 to 200 years, using the reservoir inflow discharge, for two reservoir geometry cases (stationary AEC and dynamic-updated AEC) and two conditions (empty and full). These

simulations showed that incorporating updated reservoir geometry significantly affected peak outflow discharge, released flood volume, and maximum reservoir water level. For the 200-year flood under empty-reservoir conditions, the dynamic-geometry scenario produced a peak outflow approximately 144 m^3/s higher and a released flood volume about 12 million m^3 greater than those obtained under the stationary-geometry scenario. Maximum reservoir water levels also increased by up to 45 cm for floods with smaller return periods. These results indicate that reservoir morphological evolution can substantially affect flood routing performance and flood risk estimates. The integration of Sentinel-2 imagery with Google Earth Engine provides a rapid, cost-effective, and repeatable framework for updating reservoir geometry and reducing uncertainty in flood-routing studies. The proposed methodology offers a practical tool for reservoir operation, dam safety assessment, and adaptive flood management in sediment-affected reservoirs.

Keywords: Flood routing; Reservoir sedimentation; Reservoir morphology; Sentinel-2; Google Earth Engine; Golestan Dam Reservoir.

1. Introduction

Reservoirs are among the most important components of water-resources infrastructure worldwide, serving a wide range of functions including domestic, agricultural, and industrial water supply, hydropower generation, and support of riverine ecosystems. They also play a critical role in flood management by temporarily storing floodwater and attenuating incoming flood hydrographs. Through appropriate operation, reservoirs can reduce peak discharges, delay flood-wave propagation, and lessen downstream economic and social impacts (Elfeki et al., 2020; Boulange et al., 2021; Zhao et al., 2022). In the context of increasing hydrological extremes associated with climate change (Algeria et al., 2024), reliable evaluation of reservoir performance under flood conditions has become increasingly important.

Flood routing is widely applied to assess the hydrological behavior and flood-control performance of reservoirs. Its accuracy depends on several factors, including watershed characteristics, inflow hydrographs, outlet structures, and reservoir geometry (Kim et al., 2022). Among these, the AECs and storage–elevation curves (SECs) are particularly important because they determine the available storage capacity at different water levels and directly govern the storage–release process during flood events. Since reservoir water surface area is a fundamental variable in flood routing calculations, changes in this parameter can significantly affect reservoir response.

Despite the importance of reservoir geometry, most flood-routing studies and operational analyses assume that AECs and SECs remain constant throughout a reservoir's life. While this assumption simplifies the routing procedure, it rarely reflects actual reservoir conditions. Sediment transported from upstream catchments is continuously deposited within reservoirs, leading to gradual changes in bed morphology, loss of storage capacity, and alteration of the original geometric relationships. As a result, assuming a fixed reservoir geometry may introduce considerable uncertainty into estimates of storage volume, flood-mitigation performance, and routing results.

The conventional representation of reservoir geometry is based on the area–elevation relationship, which defines the water surface area corresponding to each reservoir water level. This relationship is controlled by reservoir bathymetry and is generally established during the design and commissioning stages using hydrographic survey data. Over time, however, repeated flood events and continuous sediment deposition modify reservoir-bed topography and gradually alter the original AEC. Consequently, the water surface area associated with a given water level may differ substantially from the original design condition as sediment accumulates within the reservoir (Figure 1). Recent studies have emphasized the importance of considering these changes in reservoir analyses. Ma et al. (2025) showed that reliance on outdated SECs may result in substantial underestimation of flood risk and reservoir flood-control performance. Likewise, Zhou et al. (2024) reported that progressive sediment accumulation within the flood-control storage zone of the Three Gorges Reservoir reduces its capacity to regulate flood flows. Ren et al. (2024) highlighted the strong interaction between sediment transport processes and reservoir hydrological performance, demonstrating that sediment-driven morphological changes can significantly influence reservoir responses to flood inflows. In addition, geomorphological studies of large reservoirs have shown that long-term morphological evolution may substantially alter the geometry assumed during the design stage (Pogorelov et al., 2024).

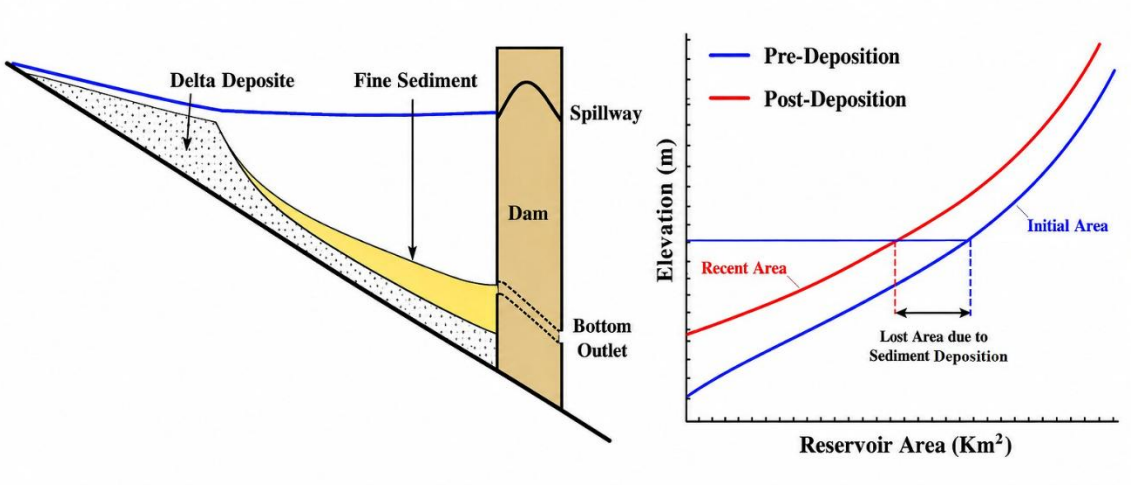


Figure 1. Schematic representation of sedimentation effects on the reservoir area–elevation curve.

These findings underscore the need for continuous monitoring of reservoir geometry and periodic revision of AECs and SECs. Traditionally, such information has been obtained through hydrographic and bathymetric surveys. Although these methods provide reliable measurements, their application in large reservoirs is often costly, labor-intensive, and time-consuming, which limits their routine use in many regions of the world (Foteh et al., 2018; Schwatke et al., 2021; Lai et al., 2024). Consequently, many reservoirs still lack updated information on storage capacity loss and long-term geometric evolution because of operational and financial limitations (Singh et al., 2025).

Over the last two decades, advances in remote sensing and the growing availability of satellite imagery with improved spatial and temporal resolution have opened new opportunities for reservoir monitoring. Numerous studies have demonstrated that Landsat and Sentinel-2 imagery, together with spectral water indices such as the Normalized Difference Water Index (NDWI) and Modified NDWI (MNDWI), can effectively delineate water boundaries and track temporal variations in reservoir surface area (Du et al., 2016; Zhou et al., 2017; Ji et al., 2009; Khalifeh et al., 2019). Other studies have shown that combining remote sensing observations with cloud-computing platforms such as Google Earth Engine (GEE) enables automated monitoring of reservoir surface area, storage volume, and long-term dynamics at both regional and global scales (Schwatke et al., 2021; Condeça et al., 2022; Chagas et al., 2025).

Beyond monitoring surface-area variations, several studies have used satellite observations to reconstruct reservoir geometric relationships and assess changes in storage capacity. Avisse et al. (2017), Liu et al. (2022), and Mahato et al. (2025) demonstrated that integrating optical imagery,

satellite altimetry, and digital elevation models (DEMs) can provide valuable information on reservoir-capacity variations. Schwatke et al. (2021) developed an automated framework for extracting reservoir water levels and surface areas from multi-temporal Landsat and Sentinel-2 observations. They showed that long-term shoreline dynamics can reveal important aspects of reservoir geometric evolution. Similarly, Ma et al. (2025) proposed approaches to update SECs affected by reservoir's sedimentation and demonstrated that neglecting these changes can lead to significant underestimation of flood-management risks and downstream hazards. In addition, remote sensing techniques have been widely applied to monitor reservoir water-quality variables, including water temperature, chlorophyll-a, turbidity, salinity, and nutrient concentrations, particularly where field measurements are expensive or difficult to obtain (Adjovu et al., 2023, Nikoo et al., 2024). Despite these advances, most previous studies have focused primarily on estimating reservoir surface area, water level, storage volume, or water quality, whereas the hydrological consequences of reservoir morphological evolution have received comparatively limited attention. Although remote sensing techniques can now detect geometric changes with reasonable accuracy, the extent to which such changes affect flood-routing simulations, flood-control performance, and downstream outflow hydrographs remains insufficiently explored (Xiaoyan et al., 2023; Suresh et al., 2024; Ma et al., 2025). Furthermore, many flood-routing studies still rely on stationary geometry assumptions derived from original design curves, without accounting for progressive changes occurring during reservoir operation. Accordingly, a significant research gap remains at the intersection of remote sensing–based reservoir monitoring and flood-routing analysis. This study addresses that gap by quantifying the effects of sediment-induced morphological changes on flood routing results by updating reservoir's AECs. The proposed framework allows continuous monitoring of reservoir surface-area variations while incorporating updated geometric information into flood-routing analyses.

The Golestan Dam Reservoir in northeastern Iran was selected as the case study. The Gorganrud River watershed is prone to intense rainfall events and flash floods, which expose the reservoir to overtopping risks and increase downstream flood hazards. The presence of extensive agricultural areas downstream further highlights the importance of reliable flood-routing assessments. Historical floods in 2001, 2002, 2005, and 2019 illustrate the watershed's high flood potential. Despite these major flood events, no dedicated flood-control storage has been allocated within the reservoir.

In this study, updated AECs for the Golestan Dam Reservoir were derived from Sentinel-2 imagery using the NDWI index in Google Earth Engine. These updated geometric curves were then incorporated into reservoir flood-routing simulations. Specifically, this study seeks to answer the following questions:

(1) How has sedimentation-driven morphological evolution affected the AECs of the Golestan Dam Reservoir?

(2) How do these geometric changes influence flood-routing performance and outflow hydrograph characteristics?

and (3) To what extent can remotely updated AECs improve the assessment of reservoir flood-control performance?

The results are expected to contribute to the integration of remote sensing into reservoir hydrology and to improve understanding of the implications of sedimentation for flood management and downstream flood-risk reduction.

2. Materials and Methods

2.1. Study Area

Built between 1995 and 1999, the Golestan dam was completed in 1999. This 25 m high dam was designed as a homogeneous earth-fill dam. The original volume of the reservoir was 86500000 m^3. Golestan Dam is one of the major embankment dams in northeastern Iran, located in Golestan Province near Gonbad Kavus City. Constructed across the Gorganrud River, the dam primarily serves agricultural water supply and domestic water demands in the region. Geographically, the dam is situated at 55°10′ E longitude and 37°22′ N latitude. Figure 2 illustrates the geographical location of the dam, the reservoir, and its major hydraulic components, including the dam body, spillway, and bottom outlet structures. The spillway with an effective crest length of 110 m and

discharge coefficient of 1.7, releases flood discharge from the dam reservoir at a maximum flow rate of 1500 m^3/s.

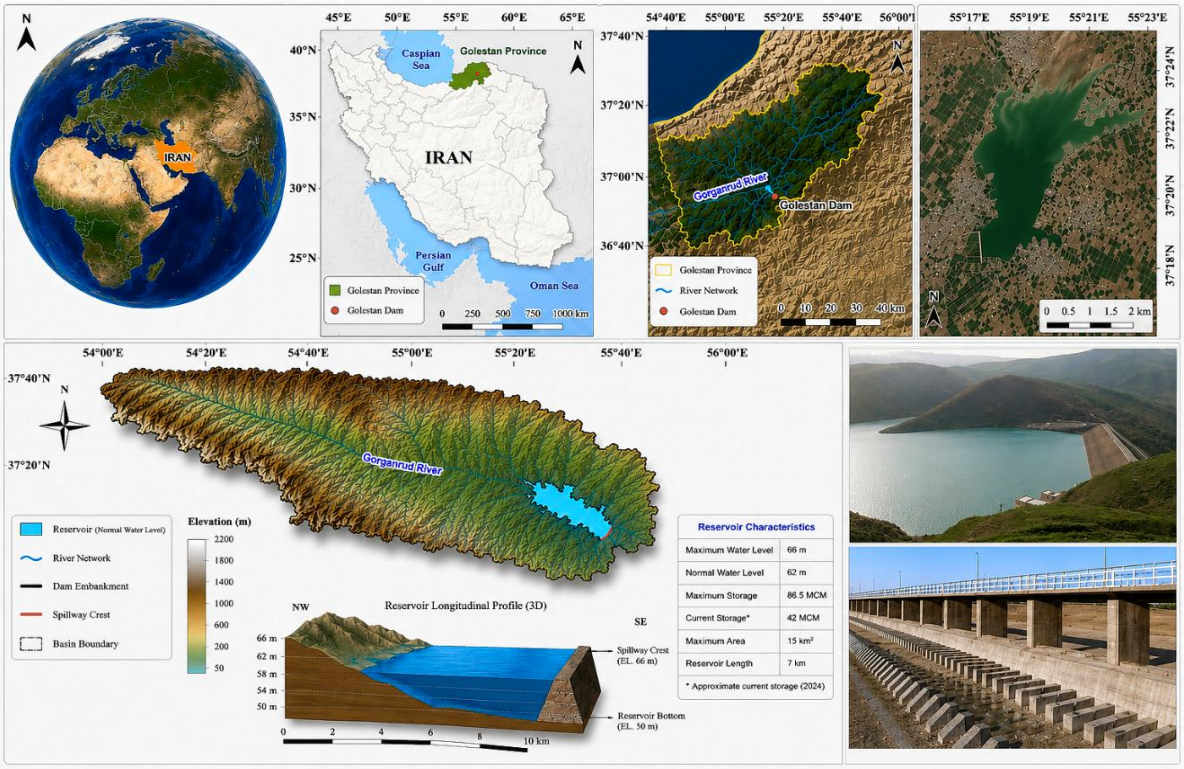


Figure 2. Location of Golestan Dam on the Gorganrud River and its main components, including the dam body and spillway.

2.2. Satellite Data and Google Earth Engine Platform

Google Earth Engine (GEE) is a cloud-based geospatial analysis platform that provides access to large archives of remote sensing imagery and environmental datasets. The platform hosts a wide range of data sources, including Landsat, Sentinel-1, Sentinel-2, MODIS, CHIRPS climate products, digital elevation models (DEMs), and various meteorological datasets. Because data processing is performed within a cloud-computing environment, large-scale analyses can be conducted efficiently without the need for high-performance local computing facilities.

In this study, Sentinel-2 imagery was used to derive the water surface area of the Golestan Dam Reservoir. The workflow included image acquisition for the study area and selected periods, cloud filtering based on image-quality indicators, and selecting scenes with minimal cloud contamination (Kaplan & Advan, 2017). The Normalized Difference Water Index (NDWI) was then calculated to

delineate the reservoir water surface, and the corresponding water area was estimated in square kilometers. A schematic representation of the methodology is provided in Figure 3.

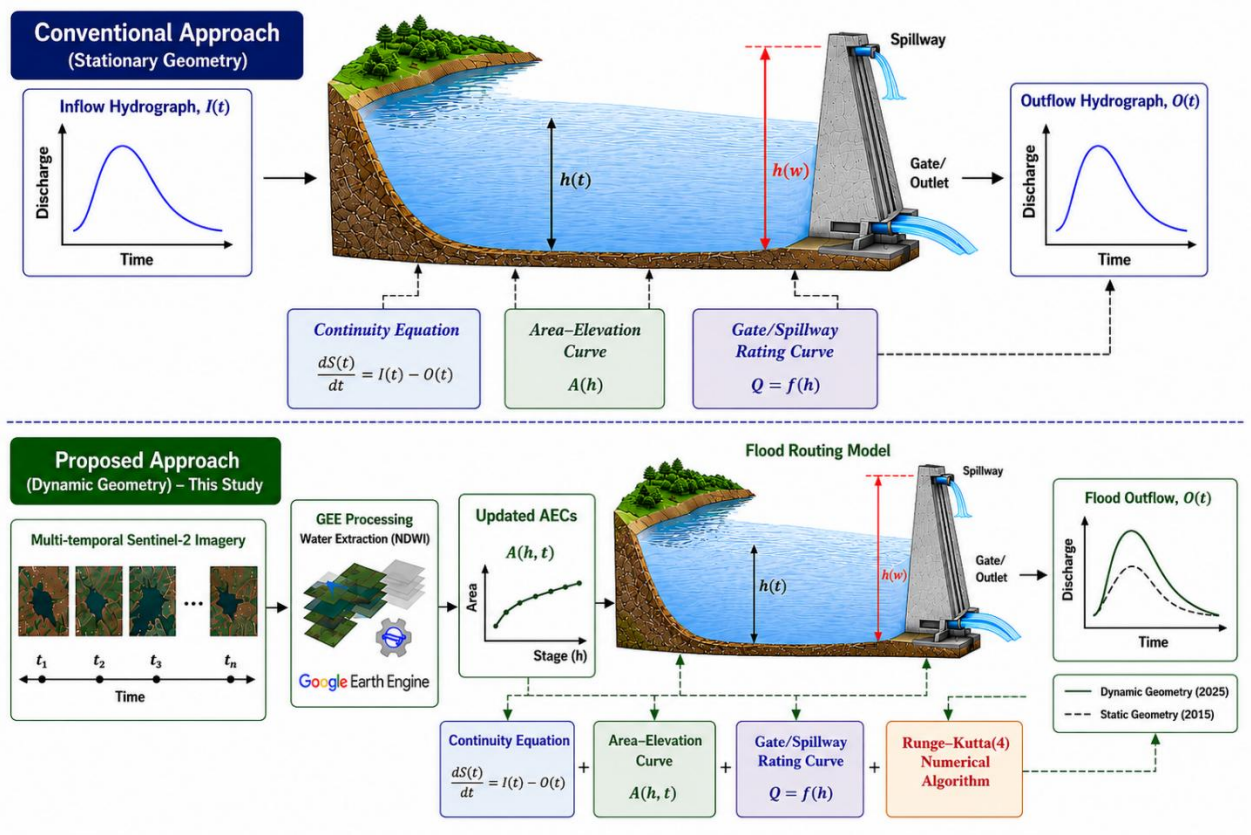


Figure 3. Components of flood routing in dam reservoirs.

Before the launch of Sentinel-2, MODIS products were commonly employed for surface-water monitoring because of their high temporal resolution (1–2 days) (Verpoorter et al., 2012). However, their relatively coarse spatial resolution (250 m) restricted their use in small reservoirs and detailed hydrological applications. Landsat imagery improved spatial resolution to 30 m but was limited by a 16-day revisit interval. Since 2015, the Sentinel-2 mission operated by the European Space Agency (ESA) has considerably improved surface-water monitoring by providing imagery with 10-m spatial resolution in the visible and near-infrared bands and a revisit frequency of approximately five days.

For water–land classification, the NDWI proposed by McFeeters (1996) was selected as the primary water-extraction index. This choice was based on its demonstrated ability to delineate water bodies accurately from Sentinel-2 imagery while preserving the dataset's native 10-m spatial resolution. Previous studies have reported reliable water-extraction performance using NDWI

without the need for additional spectral indices. Although the Modified Normalized Difference Water Index (MNDWI) (Xu, 2006) has been suggested as an alternative approach, its application requires shortwave infrared (SWIR) bands, which are available at lower spatial resolution and may reduce the spatial precision of shoreline delineation. Earlier investigations have also shown that NDWI generally provides satisfactory results, with extraction errors typically below 5%, making it suitable for the flood-routing analyses conducted in this study (Zhou et al., 2017; Chagas et al., 2025; Che et al., 2025; Mahmood et al., 2025). The NDWI index is calculated as follows:

$$\mathrm{NDWI} = \frac{\rho_{Green} - \rho_{NIR}}{\rho_{Green} + \rho_{NIR}} \tag{1}$$

where *Green* and *NIR* represent the reflectance values of the green and near-infrared spectral bands, respectively.

2.3. Reservoir Flood Routing Model

Reservoirs mitigate downstream flood hazards by temporarily storing incoming floodwaters and releasing them gradually through spillways and outlet structures (Nematollahi et al., 2024). Assessing this flood-control function requires reliable flood-routing analyses that can represent the temporal variation in inflow, outflow, and reservoir storage. Reservoir flood routing is primarily based on the continuity equation, which describes changes in storage as a function of the difference between inflow and outflow discharges (Figure 4). Among the available routing methods, the Modified Puls method, also known as level-pool routing, is one of the most commonly used techniques in reservoir-routing applications (Arrieta-Pastrana et al., 2024). Thismethod assumes a horizontal water surface within the reservoir and is therefore particularly suitable for reservoirs with small water-surface gradients. In reservoirs with elongated geometry and pronounced water-surface profiles, hydraulic-routing approaches may be more appropriate.

Application of the Modified Puls method typically requires an inflow hydrograph, outlet rating curves, and the reservoir SEC. In many cases, however, updated SECs are not available because hydrographic and bathymetric surveys are costly and conducted only at relatively long intervals. As a result, SECs are often derived indirectly from AECs, introducing an additional source of uncertainty into the routing procedure. To reduce this uncertainty, the present study adopts a flood-routing framework that directly incorporates AECs derived from satellite observations, thereby avoiding the intermediate conversion to SECs. The governing differential equation can be expressed as:

$$\frac{dh}{dt} = \frac{I(t) - O_{out}(h)}{A(h)} \tag{2}$$

$$O_{out} = O_{weir} + O_{gate} = C_w L_w (h - h_w)^{1.5} + C_g A_g \sqrt{2gh} \tag{3}$$

where h is the reservoir water level, $A(h)$ denotes the reservoir surface area corresponding to water level h, $I(t)$ represents the inflow flood hydrograph, $O_{out}(h)$ is the total outflow discharge from the reservoir which is calculated as the sum of spillway discharge (O_{weir}) and bottom outlet release (O_{gate}), C_w is the spillway discharge coefficient, L_w is the effective spillway crest length, h_w is the spillway crest elevation, C_g is the outlet discharge coefficient, A_g is the bottom outlet opening area, and g is the gravitational acceleration. The function $A(h)$ is not constant through time. Sediment deposition from repeated flood events gradually alters reservoir morphology and reduces the reservoir surface area at a given water level. If these geometric changes are ignored, flood-routing results, including peak reservoir levels and outflow hydrographs, may be significantly biased. Because accurate estimation of the maximum reservoir water level and spillway discharge is essential for dam safety assessment and downstream flood risk management, updated AECs were incorporated into the flood routing model. Reservoir surface areas corresponding to different water levels were derived directly from Sentinel-2 imagery and subsequently integrated into the flood routing framework. The governing ordinary differential equation was solved numerically using the fourth-order Runge–Kutta method. This approach was selected for its high numerical accuracy and computational efficiency in solving initial-value problems in reservoir-routing simulations.

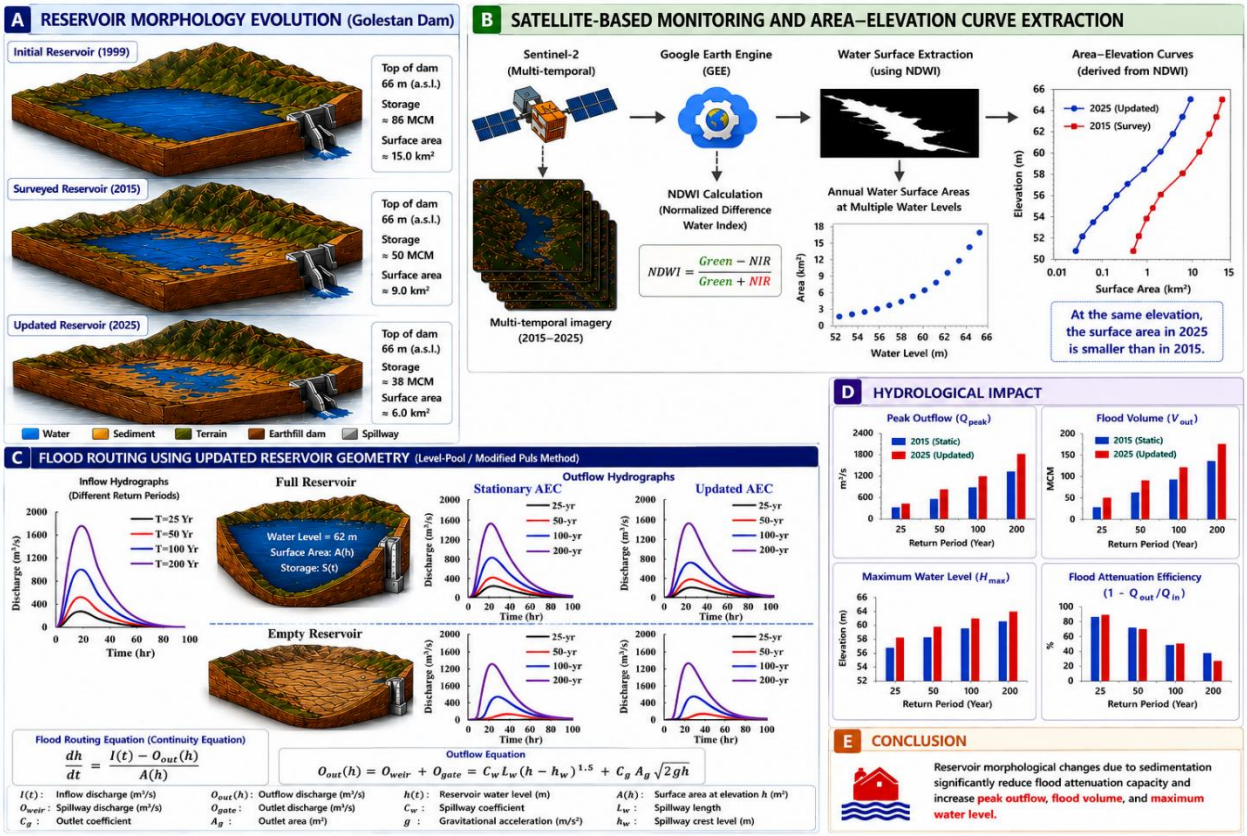
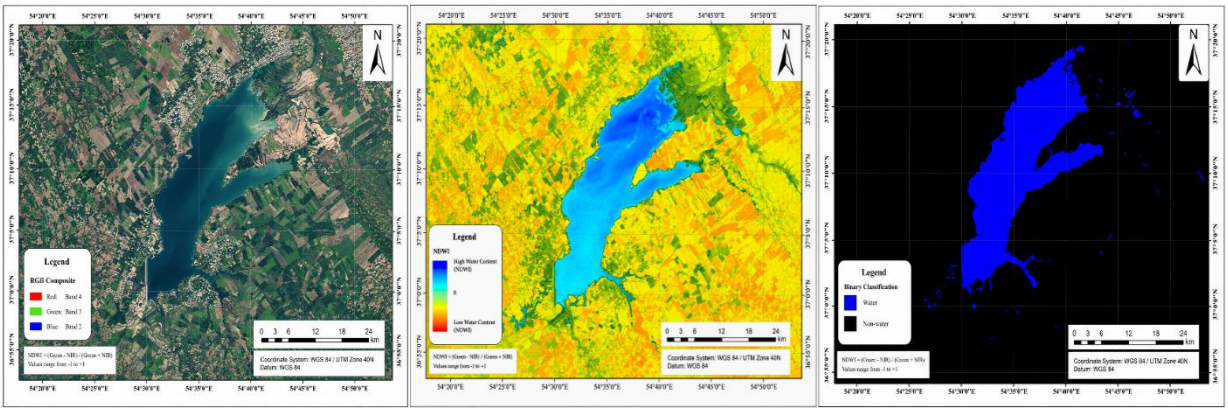


Figure 4. Flowchart of reservoir flood routing based on remotely sensed stage–area curve updating.

4. Results

4.1. Extraction of Reservoir Surface Area Using Sentinel-2 Imagery

The workflow developed within the GEE environment was applied to estimate the reservoir surface area at different water levels in the Golestan Reservoir. For this purpose, more than 100 Sentinel-2 images acquired between 2015 and 2025 were processed. Image acquisition dates were selected to ensure that the corresponding reservoir water levels covered a representative elevation range of approximately 55.5–63 m. An example of the processing sequence used to extract the reservoir water body from Sentinel-2 imagery is shown in Figure 5, which illustrates the main steps of the proposed methodology.



(a) (b) (c)

Figure 5. Workflow of water surface area extraction in Golestan Dam Reservoir using Sentinel-2 imagery: (a) RGB satellite image, (b) water body delineation using the NDWI, and (c) binary water surface map.

Golestan Reservoir was surveyed hydrographically in 2015, approximately 16 years after the dam became operational. The survey results showed that storage capacity at the spillway crest elevation (62 m) had declined from about 86.5 million m³ in 1999 to nearly 51 million m³ in 2015, indicating a storage loss of approximately 40% as a result of sediment accumulation. During the same period, the reservoir bed elevation increased from roughly 50 m to 55.5 m (Figure 6). This figure compares reservoir surface areas derived from the proposed satellite-based approach with those from the 2015 hydrographic survey. Noticeable differences can be observed between the two AECs. These differences are not uniformly distributed across the elevation range; rather, they vary with the reservoir's hydraulic and geometric characteristics. Within the intermediate elevation range, where reservoir geometry remains relatively stable and inundation of gently sloping marginal areas is limited, the agreement between satellite-derived estimates and hydrographic observations is considerably better. Under these conditions, the hydrographic relationship appears to represent reservoir geometry with reasonable accuracy. At lower and higher water levels, however, the discrepancies become more pronounced. The root mean square error (RMSE) increases from approximately 0.56 km² in the intermediate elevation range to about 1.34 km² at lower elevations and exceeds 3 km² near the spillway crest. This pattern indicates that uncertainty in the hydrographic estimates is strongly influenced by hydraulic conditions and by the geometric sensitivity of the reservoir near its operational limits. A plausible explanation for the larger discrepancies observed at higher elevations is related to the timing of the hydrographic survey. Because the survey was conducted when the reservoir water level was approximately 57 m, the elevation–area values above this level were likely estimated through extrapolation rather than direct measurement. The nearly linear trend exhibited by the hydrographic AEC above 57 m is consistent

with this interpretation. However, reservoir's AECs generally exhibit nonlinear and often power-law characteristics (Juskula et al., 2019; Zhao et al., 2022; Schwatke et al., 2021; Yao et al., 2023; Ma et al., 2025), a pattern that is clearly captured by the GEE-derived estimates. At lower water levels, the observed differences appear to be governed by a different process. Hydrographic surveys typically represent reservoir geometry based on measurements collected at discrete locations, with spatial coverage determined by survey density, reservoir size, and sedimentation patterns. In reservoirs with significant sediment deposition, shallow areas may become partially filled, while deeper depressions continue to retain water, resulting in isolated water bodies and irregular inundation patterns. Such localized features may not be fully captured during hydrographic surveys, potentially leading to underestimation of the actual water-covered area. As a result, portions of the reservoir may be interpreted as dry despite containing measurable volumes of stored water. Satellite imagery, by contrast, records the actual water extent at the time of acquisition and can therefore detect these residual water bodies. Consequently, the satellite-based approach may provide a more realistic representation of reservoir surface area under low-water conditions (Xia et al., 2024). This issue is particularly relevant for reservoir operation during drought periods, where inaccuracies in water-surface area estimation can propagate into errors in effective storage assessment and water-allocation decisions.

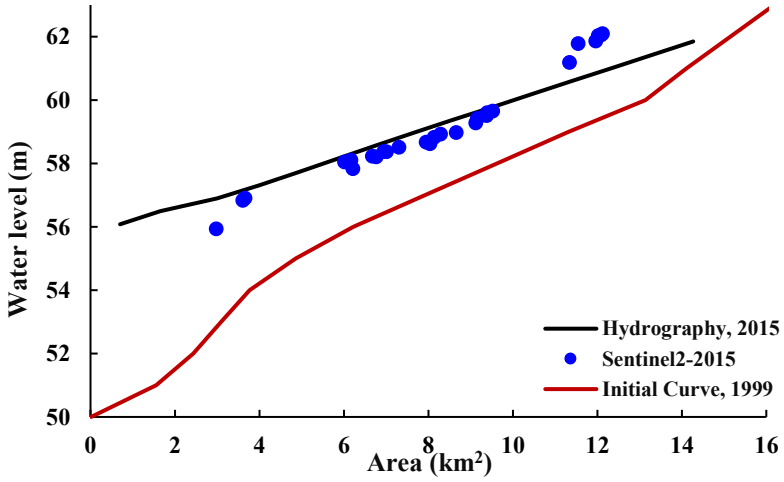


Figure 6. Comparison of the Golestan Dam Reservoir area–elevation curves obtained from the GEE algorithm and hydrographic survey data (2015).

Figure 7 presents the reservoir surface areas derived from the GEE algorithm for the period 2015–2025, together with the original design curve for 1999. The results consistently demonstrate

nonlinear behavior at both high and low elevations, suggesting that the linear assumptions commonly used in hydrographic reconstructions may not adequately capture the reservoir's geometric characteristics. These results were subsequently used to reconstruct updated AECs, as shown in Figure 8.

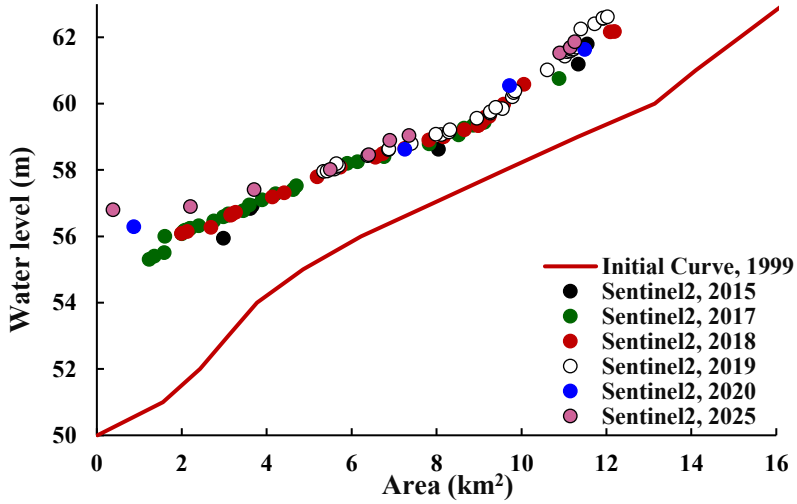


Figure 7. Changes in the Golestan Dam Reservoir water surface area during 2015–2025 and comparison with the initial AEC.

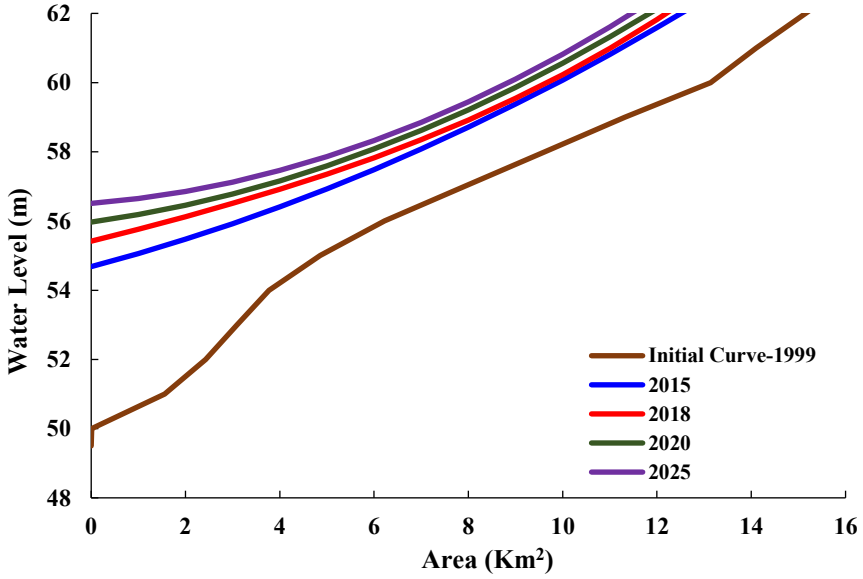


Figure 8. Extraction of reservoir AECs for the Golestan Dam Reservoir during 2015–2025 and comparison with the initial reservoir AEC.

Table 1. Percentage reduction in reservoir water surface area at different elevations of the Golestan Dam Reservoir during 2015–2025.

Water Level (m)	Surface Area (km^2)		Reduced Area (%)
	2015	2025	
55	0.93	0	100
56	3.17	0	100
57	5	2.6	48
58	6.86	5.32	22.45
59	8.45	7.26	14.08
60	9.89	8.89	10.16
61	11.25	10.24	8.98
62	12.52	11.48	8.31

4.2. Design Flood Hydrographs

Figure 9 shows the inflow flood hydrographs associated with return periods of 25-, 50-, 100-, and 200- years for the Golestan Reservoir. These hydrographs were developed using annual maximum instantaneous discharge records from the Tamar hydrometric station, located upstream of the reservoir in combination with the physiographic characteristics of the Gorganrud watershed. The estimated peak discharges of the design floods are approximately 278, 528, 991, and 1852 m^3s^{-1} for return periods of 25-, 50-, 100-, and 200- years, respectively.

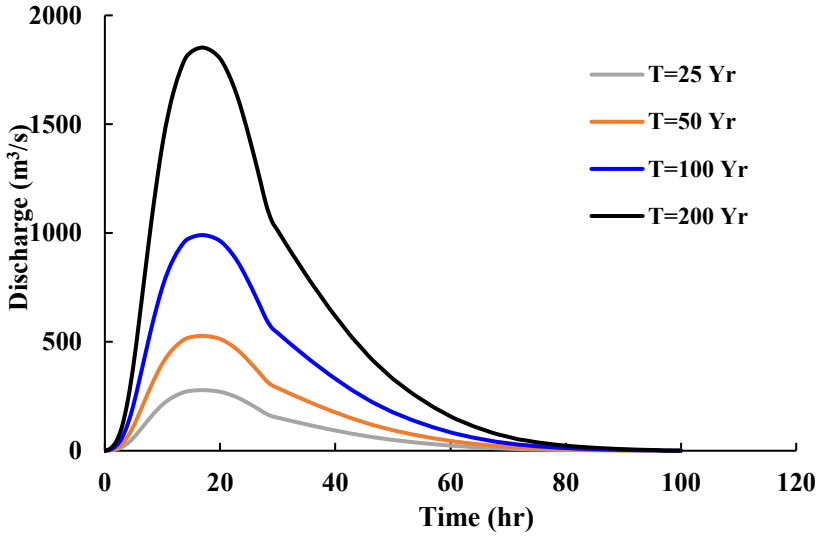


Figure 9. Inflow flood hydrographs to the Golestan Dam Reservoir for return periods ranging from 10 to 200 years.

4.3. Model Validation Using the 2001 Extreme Flood Event

The proposed flood-routing model was validated using the August 2001 flood, the most severe flood event recorded in the Gorganrud Basin. The event produced a peak inflow discharge of approximately 3020 m^3s^{-1} and entered the reservoir within a relatively short period. It was triggered by an intense storm that generated nearly 450 mm of rainfall over a 12-hour duration and resulted in extensive economic and human losses (410 fatalities). Fortunately, the flood occurred shortly after reservoir impoundment, when the reservoir was nearly empty and retained its full design storage capacity of approximately 86.5 million m^3. Under these conditions, the reservoir effectively attenuated the flood wave and prevented severe flooding in downstream urban areas, including Gonbad Kavus, Aqqala, and Gomishan.

For model validation, the observed inflow hydrograph of the 2001 event was used as the routing input. Because the flood occurred during the initial years of reservoir operation, the original 1999 AEC was adopted. Sediment accumulation during this period was considered negligible, and the original reservoir geometry was therefore assumed to remain unchanged. Based on the pre-impoundment topographic survey, the reservoir bed elevation was approximately 50 m, and the initial reservoir water level was set at 50.5 m.

Figure 10 compares the simulated and observed outflow hydrographs. The close agreement between the two hydrographs demonstrates the proposed framework's ability to reproduce the reservoir's routing behavior with satisfactory accuracy. The simulated peak outflow discharge was approximately 220 m^3s^{-1}, equivalent to only about 7% of the peak inflow discharge. The total inflow and outflow flood volumes were estimated at approximately 87 and 16.5 million m^3, respectively, indicating that more than 71% of the incoming flood volume was temporarily retained within the reservoir during the event.

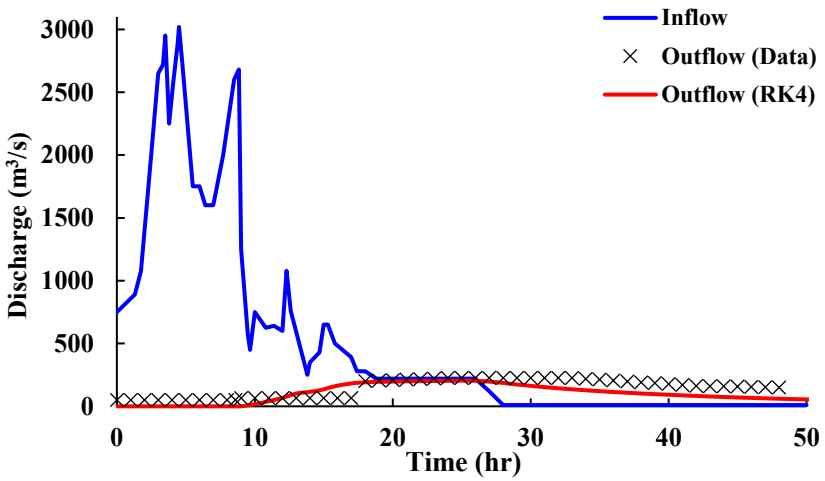


Figure 10. Flood routing results for the 2001 flood event in the Golestan Dam Reservoir using the fourth-order Runge–Kutta method.

4.4. Flood Routing under Stationary Reservoir Geometry Conditions

The flood-routing simulations conducted using the 2015 reservoir (stationary) geometry are presented in Figure 11 for design floods with return periods of 25-, 50-, 100-, and 200-years under both empty and full reservoir conditions. The corresponding quantitative results are summarized in Table 2.

The results demonstrate that reservoir storage contributes significantly to flood attenuation even when the reservoir is initially full. However, the effectiveness of flood mitigation decreases as flood magnitude increases. Specifically, for the 25-, 50-, 100-, and 200-year flood events, reductions in peak inflow discharge under full-reservoir conditions were approximately 34.9%, 28.1%, 21.9%, and 18.8%, respectively. Under empty-reservoir conditions, the attenuation capacity was substantially greater. The 25-year flood was completely retained within the reservoir, resulting in a 100% reduction in peak discharge. For the 50-, 100-, and 200-year floods, peak discharge reductions were approximately 84.4%, 53.6%, and 34.3%, respectively. These values are considerably higher than those obtained under full-reservoir conditions, highlighting the critical role of available storage capacity in flood mitigation.

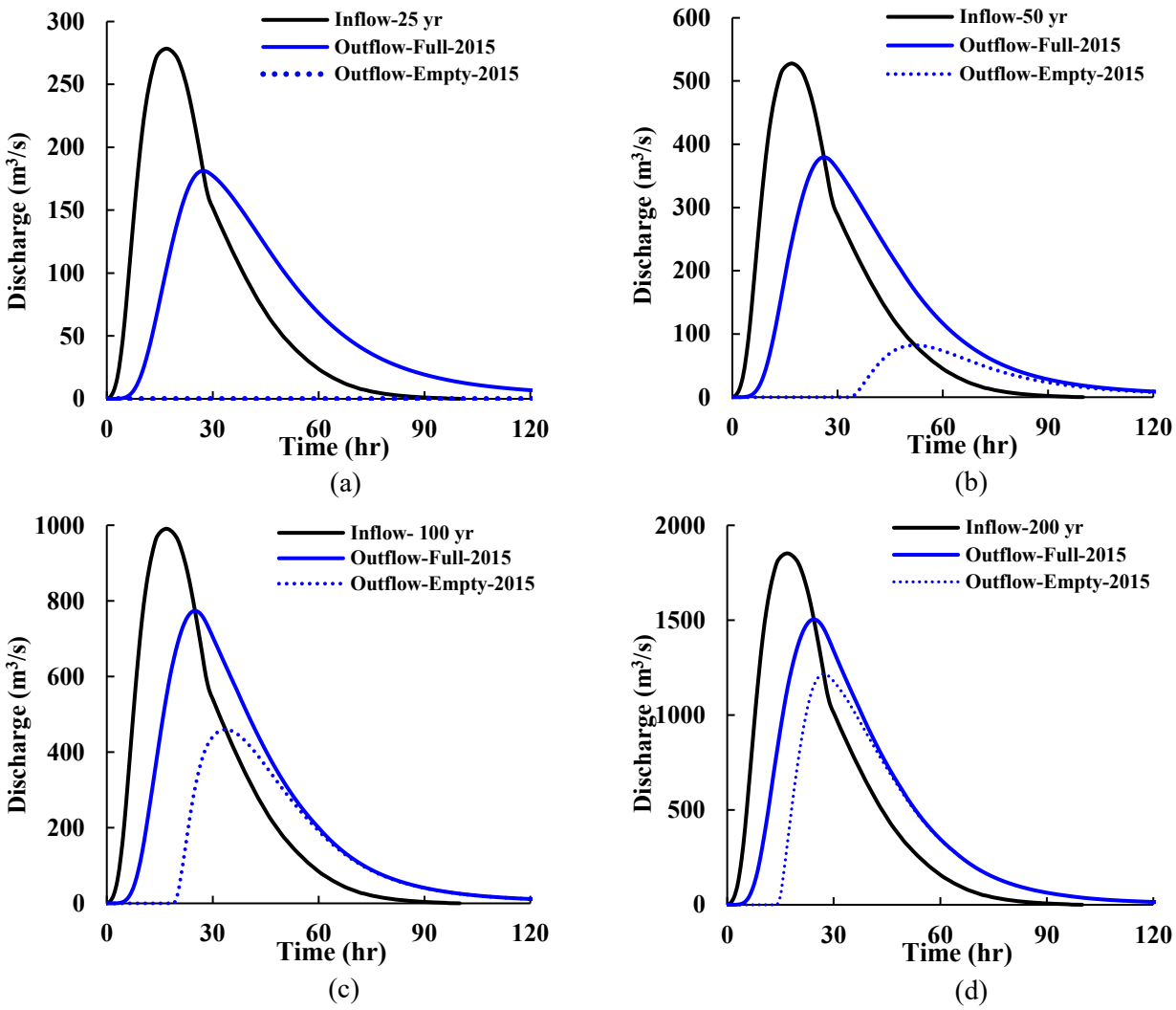


Figure 11. Flood routing results for inflow hydrographs with different return periods in the Golestan Dam Reservoir under empty and full reservoir conditions using the stationary geometry scenario (2015 area–elevation curve): (a) 25-year, (b) 50-year, (c) 100-year, and (d) 200-year floods.

A similar trend is evident in the flood-volume analysis (Table 3). For an initially empty reservoir, reductions in total flood volume were approximately 100%, 76.7%, 40.2%, and 22.8% for the 25-, 50-, 100-, and 200-year events, respectively. In contrast, volume reductions under full-reservoir conditions were negligible, reflecting the fundamental principle of mass conservation and the limited storage available for additional flood retention. These findings confirm that reservoir operation status strongly influences flood-routing performance and that available flood-control storage becomes increasingly important as flood magnitude increases.

4.5. Impacts of Morphological Changes on Flood Routing Performance

To assess the hydrological consequences of sediment-induced morphological evolution, flood-routing simulations were performed using both the stationary and the updated AECs derived from Sentinel-2 observations for 2015 and 2025, respectivly. The resulting outflow hydrographs are shown in Figure 12. The results indicate that accounting for morphological changes significantly influences reservoir-routing behavior. Compared with the stationary geometry, the updated geometry produces higher peak outflow discharges, larger released flood volumes, and noticeable modifications in hydrograph shape. These effects are most evident for smaller return-period floods and when the reservoir is initially empty. For example, during the 50-year flood under empty-reservoir conditions, the simulated peak outflow increased from 82.1 m^3s^{-1} to 131.3 m^3s^{-1}, representing an increase of approximately 49 m^3s^{-1} or about 9.3% of the inflow peak discharge. Under full-reservoir conditions, the corresponding increase was limited to approximately 12m^3s^{-1}. For the 100 and 200-year floods, peak outflow increases under empty-reservoir conditions reached approximately 63.5 m^3s^{-1} (6.4% of the inflow peak) and 144 m^3s^{-1} (7.8% of the inflow peak), respectively. These results suggest that sediment accumulation and the resulting loss of effective storage capacity progressively reduce the reservoir's flood-attenuation capability. A similar pattern is observed in the volume-based analysis. Using the updated geometry under empty-reservoir conditions, reductions in flood volume relative to inflow volume were approximately 100%, 65.2%, 34.2%, and 17.0% for the 25-, 50-, 100-, and 200-year floods, respectively. Relative to the values obtained with the updated geometry, these results indicate a decline of roughly 6–11% in flood-retention performance. The implications of these differences are operationally significant. During the 200-year flood, for example, the routed outflow volume increased from approximately 149 million m^3 under the 2015 geometry to about 161 million m^3 under the updated geometry, resulting in an additional downstream release of nearly 12 million m^3 of floodwater. Such increases may substantially raise the risk of flooding and potential damage in downstream floodplains and densely populated areas. Overall, the results show that the use of outdated reservoir geometry may lead to underestimation of downstream flood hazards while simultaneously overestimating reservoir flood-control performance. Periodic updating of reservoir geometric relationships is therefore essential for improving the reliability of flood-risk assessments and reservoir-operation analyses.

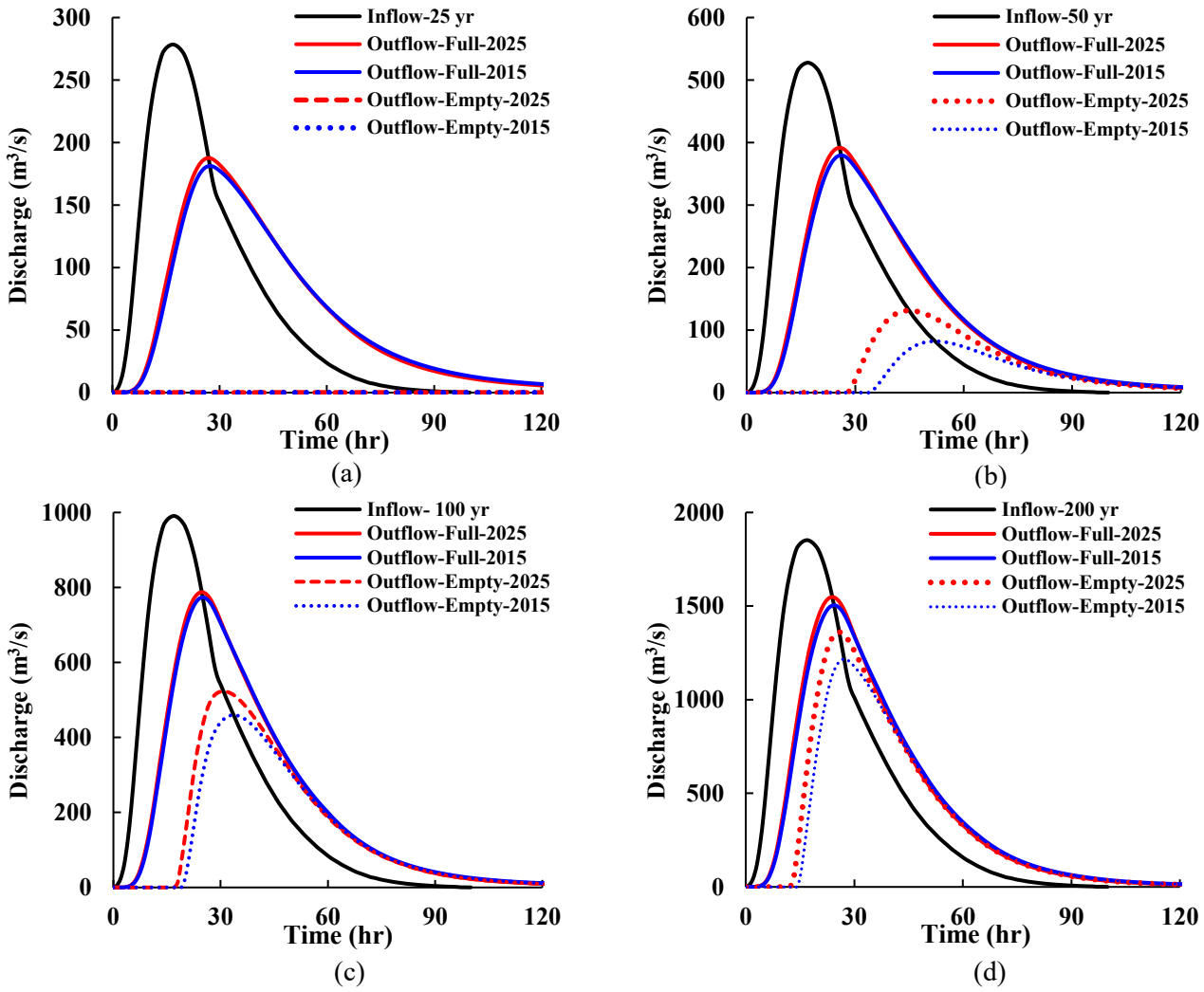


Figure 12. Comparison of reservoir outflow hydrographs under empty and full reservoir conditions using the 2015 and 2025 reservoir topographies: (a) 25-year, (b) 50-year, (c) 100-year, and (d) 200-year floods.

4.6. Reservoir Water-Level Response under Static and Dynamic Geometry Scenarios

Figure 13 shows the simulated reservoir water-level fluctuations for both the stationary and updated geometry scenarios, with initial conditions of full and empty reservoirs. During the 25-year flood under empty-reservoir conditions, the maximum water level remained below the spillway crest elevation in both scenarios, indicating that the incoming flood volume could be fully accommodated within the reservoir. In contrast, for the 200-year flood under full-reservoir conditions, the simulated maximum water level approached the dam crest elevation (66 m) across all geometry scenarios. Considering that Golestan Dam is an earth-fill dam, such conditions may represent a critical safety concern. The simulations further suggest that flood events with a 200-

year return period could substantially reduce available freeboard and potentially threaten dam safety. This issue is not limited to full-reservoir conditions and may also become relevant when the reservoir is initially empty. Although Golestan Dam is equipped with two low-level outlet gates with a combined discharge capacity of approximately 50 m^3s^{-1}, these structures were not included in the present simulations because operational limitations may restrict their effective use during extreme flood events.

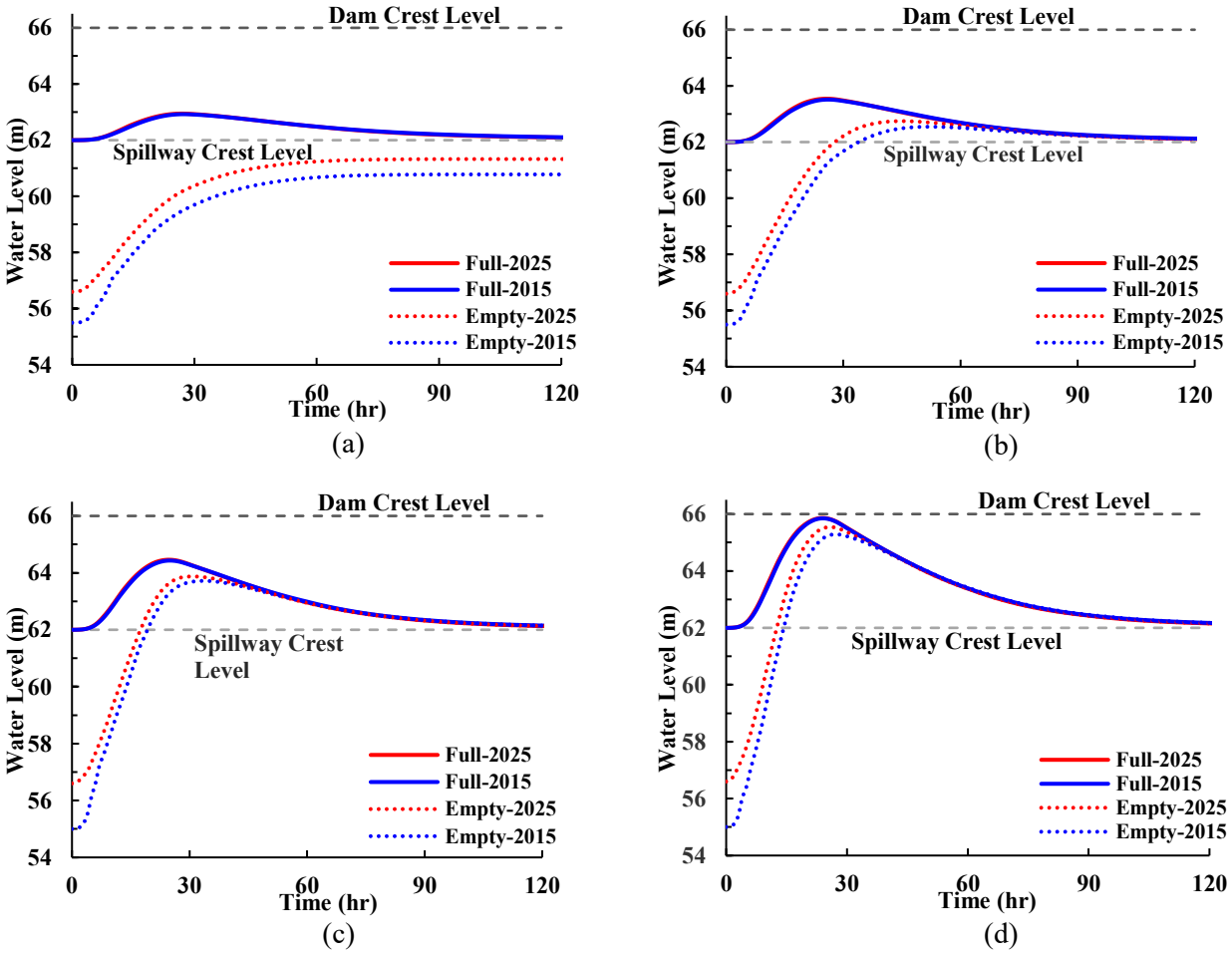


Figure 13. Reservoir water level variations obtained from routing floods with different return periods in Golestan Dam Reservoir under full and empty reservoir conditions and for the two reservoir bed topographies derived from stationary and updated AECs: (a) 25-year, (b) 50-year, (c) 100-year, and (d) 200-year return period floods.

Incorporation of the updated reservoir geometry resulted in higher simulated reservoir water levels for all flood scenarios under empty-reservoir conditions. The relative effect was particularly evident for floods with smaller return periods. Maximum water-level increases were approximately 45, 20, 18, and 17 cm for the 25-, 50-, 100-, and 200-year floods, respectively. These results

indicate that long-term sediment buildup not only influences downstream flood routing characteristics but also affects the reservoir's water-level response. From a management perspective, neglecting reservoir morphological evolution may lead to underestimation of both downstream flood hazards and maximum reservoir water levels during extreme events. Consequently, incorporating updated reservoir geometry into flood-routing analyses and reservoir-management practices is essential to improve the reliability of flood-risk assessments and support the long-term safety and effectiveness of reservoir operations.

Table 2. Simulated peak outflow discharge and percentage reduction in peak discharge for 25, 50, 100, and 200-year return period floods in Golestan Dam Reservoir under full and empty reservoir conditions and two reservoir topographies derived from the stationary and updated AECs.

T(yr)	$Q_{Peak\text{-}Inflow}$ (m^3/s)	$Q_{Peak\text{-}Outflow}$ (m^3/s)				ΔQ_P (%)			
		Stationary AEC		Updated AEC		Stationary AEC		Updated AEC	
		Empty	Full	Empty	Full	Empty	Full	Empty	Full
25	278.45	0	181.25	0	187.66	100	34.91	100	32.60
50	527.79	82.15	379.58	131.34	391.51	84.44	28.08	75.11	25.82
100	990.69	459.53	773.59	523.04	787.18	53.61	21.91	47.21	20.54
200	1852.13	1216.74	1503.30	1360.66	1548.33	34.31	18.83	26.54	16.40

Table 3. Simulated flood volumes and percentage reduction in outflow flood volume for 25, 50, 100, and 200-year return period floods in Golestan Dam Reservoir under full and empty reservoir conditions and two reservoir topographies derived from the stationary and updated AECs.

T(yr)	V_{Inflow} (mcm)	$V_{Outflow}$ (mcm)				ΔV (%)			
		Stationary AEC		Updated AEC		Stationary AEC		Updated AEC	
		Empty	Full	Empty	Full	Empty	Full	Empty	Full
25	29.08	0	28.52	0	28.71	100	1.92	100	1.27
50	55.12	12.85	54.55	19.16	54.81	76.70	1.03	65.24	0.55
100	103.47	61.85	102.99	68.06	102.99	40.22	0.46	34.22	0.45
200	193.43	149.30	193.32	160.57	193.25	22.82	0.06	16.99	0.09

5. Discussion

The comparison between AECs derived from the 2015 hydrographic survey and those reconstructed from Sentinel-2 imagery provides insights beyond a simple statistical analysis. The observed differences reflect the combined effects of sediment-driven morphological change, survey-related limitations, and the reservoir's varying hydraulic sensitivity across its operating range. Therefore, the discrepancies should not be interpreted solely as measurement errors but rather as manifestations of the different physical conditions represented by the two datasets. The results of a reservoir hydrographic survey are usually used as a benchmark for evaluating any proposed remote sensing framework. However, our comparison of Golestan Dam's reservoir

showed that agreement between the two approaches varies with water level. In the intermediate stage range, where the reservoir geometry is relatively stable and inundation of marginal areas is limited, the correspondence between hydrographic and satellite-derived estimates was generally satisfactory. By contrast, larger deviations occurred near the reservoir's extreme lower and upper operating limits, suggesting that both hydraulic conditions and geometric sensitivity strongly influence uncertainty in AECs. At higher water levels, part of the discrepancy can likely be attributed to the survey procedure. Since the hydrographic survey was conducted when the reservoir water level was as low as about 57 m, the water-surface areas above this level were likely extrapolated rather than directly measured. The nearly linear trend observed in the hydrographic data at upper elevations is consistent with this interpretation. Such behavior differs from the nonlinear patterns commonly reported for reservoir AECs, which typically reflect reservoir topography and are often described by polynomial or power functions (Schwatke et al., 2021; Yao et al., 2023; Ma et al., 2025). In contrast, the reconstructed curves from the GEE-based analysis retained this nonlinear behavior and appeared more consistent with the reservoir's expected geomorphological characteristics.

The differences observed at lower water levels are more plausibly associated with sedimentation-induced alterations of the reservoir bed. In reservoirs with substantial sediment deposition, localized depressions frequently form in the deeper portions. Such obstructions may not be fully surveyed during hydrographic surveys (Furnans & Austin, 2008) due to limitations in sampling density and spatial coverage. Satellite imagery, however, captures the actual water extent at the time of acquisition and can therefore detect these obstructions more effectively. As a result, the remotely sensed estimates may provide a more realistic representation of water surface area in low stage elevations. Beyond the differences in geometric representation, the comparison highlights several practical advantages of the proposed methodology. Hydrographic surveys provide detailed geometric information but require substantial financial resources, specialized equipment, and extensive field operations. Consequently, such surveys are generally conducted at relatively long intervals. In reservoirs experiencing rapid sediment accumulation, these intervals may cause significant divergence between the actual reservoir condition and the geometry derived from stationary AECs. Sentinel-2 imagery combined with the Google Earth Engine platform offers a rapid, repeatable, and cost-effective alternative for tracking geometric changes. Because the approach does not rely on predefined AEC, it can be applied whenever suitable imagery is available, enabling continuous monitoring of reservoir evolution through time. This capability is

particularly valuable in regions where frequent hydrographic surveys are difficult to conduct economically or operationally.

A key outcome of this study is the demonstrated influence of reservoir evolution on flood-routing behavior. Conventional routing analyses generally assume that AECs and SECs remain unchanged throughout the operational life of a reservoir. The results for the Golestan Reservoir indicate that this assumption may introduce substantial uncertainty in cases with persistent sediment accumulation. When the updated 2025 AEC was incorporated into the routing simulations, higher peak outflows, larger released flood volumes, and greater maximum reservoir water levels were obtained compared with simulations based on the stationary 2015 geometry. The effects of these geometric changes were most pronounced for smaller return-period floods under initially empty-reservoir conditions. As effective storage capacity gradually decreases due to sedimentation, a greater proportion of incoming floodwater must be released downstream, leading to higher outflow peaks and greater flood volumes. Consequently, the reservoir's flood-attenuation capacity gradually declines over time. Similar conclusions have been reported in previous studies that identified sedimentation as a major factor reducing flood-control efficiency and increasing downstream flood risk (Zhou et al., 2024; Ma et al., 2025). The routing simulations further suggest that neglecting long-term morphological change may lead to underestimation of both downstream flood hazards and dam-safety concerns. For the Golestan Dam, extreme flood events were shown to raise reservoir water levels close to the dam crest elevation. These findings underscore the importance of incorporating updated AECs into flood-routing studies and dam-safety assessments, particularly for reservoirs with substantial sediment accumulation.

Overall, the results demonstrate that integrating remote sensing observations with hydrological routing models provides an effective framework for representing time-varying reservoir conditions in flood-routing analyses. Rather than replacing hydrographic surveys, the proposed methodology should be viewed as a complementary monitoring tool capable of supplying frequent geometric updates between field campaigns. Such integration can reduce uncertainties associated with static reservoir representations and improve the reliability of flood-risk assessments, reservoir operation strategies, and long-term water-resources planning.

Although uncertainties are inherent in both the remote sensing and routing components of the proposed framework, their influence is unlikely to alter the main conclusions of this study. Potential sources of uncertainty include water-boundary extraction errors associated with image quality and cloud contamination, temporal mismatches between satellite overpasses and in situ reservoir’s

552 water-level observations, and assumptions embedded in the routing model. Nevertheless, the
553 differences observed between the stationary and dynamic geometry scenarios were substantially
554 larger than the expected magnitude of these uncertainties, indicating that the reported changes
555 primarily reflect actual reservoir morphological evolution rather than methodological artifacts.
556 Several limitations should nevertheless be acknowledged. The accuracy of the extracted water-
557 surface areas depends on image availability, cloud contamination, and the spatial resolution of
558 Sentinel-2 imagery. Furthermore, the present investigation focused on a single reservoir, and
559 application of the framework to reservoirs with different morphological settings and sedimentation
560 regimes would provide a broader basis for evaluation. Future studies may benefit from integrating
561 satellite altimetry, updated digital elevation models, and real-time reservoir operation models to
562 further improve dynamic flood routing simulations and reservoir management applications.
563
564 **6. Conclusions**
565 This study highlights the importance of accounting for reservoir morphological change in flood
566 routing analyses and demonstrates the potential of remote sensing techniques to maintain up-to-
567 date geometric information in sediment-affected reservoirs. By integrating Sentinel-2 imagery with
568 the Google Earth Engine platform, a practical framework was developed to reconstruct reservoir
569 AECs and evaluate their influence on routing simulations.
570 The comparison between AECs derived from hydrographic surveys and remote sensing showed
571 that the level of agreement varies across the reservoir operating range, with the largest differences
572 occurring near the lower and upper hydraulic limits. These results indicate that reservoir geometry
573 cannot always be represented adequately by a single static relationship, particularly in systems
574 subject to continuous sediment accumulation. Multi-temporal analysis of the Golestan Reservoir
575 revealed substantial geometric changes during the study period, confirming that sediment
576 deposition progressively modifies reservoir characteristics over time. Incorporating the updated
577 geometry into the routing simulations resulted in higher peak outflows, larger released flood
578 volumes, and higher maximum reservoir water levels than simulations based on the stationary
579 AECs. The influence of these changes was most evident under initially empty-reservoir conditions,
580 where the reduction in effective storage capacity had a greater impact on flood attenuation. The
581 results emphasize that the use of stationary geometric information may lead to underestimation of
582 downstream flood hazards and reservoir operational risks. Periodic updating of AECs and SECs

should therefore be considered an essential component of flood-risk assessment, reservoir operation, and dam-safety evaluation in sediment-prone reservoirs.

Future developments may focus on combining satellite-derived geometric information with storage estimation, sedimentation monitoring, satellite altimetry, and real-time reservoir-operation models. Such advances would support more adaptive flood-management strategies and enhance the long-term resilience of reservoir systems under changing hydrological and climatic conditions.

The results highlight the importance of moving from static toward dynamically updated reservoir representations in flood-routing studies, particularly in sediment-prone reservoirs where geometric evolution can substantially alter flood-control performance.

7. Funding

This work was funded by national funds through Gorgan University of Agricultural Sciences and Natural Resources (GUSNR) under grant no. 235646. The authors therefore acknowledge GUSNR with thanks for financial support. The authors also gratefully acknowledge the Golestan Regional Water Authority for providing reservoir water-level records and hydrographic survey data used in this study. The Sultan Qaboos University research group DR/RG/28: “Climate Change, Water, and Environmental Modeling” is gratefully acknowledged. Sentinel-2 imagery employed in this research was obtained through the Copernicus Programme and processed using the Google Earth Engine (GEE) cloud-computing platform.

8. Author Contributions

Abdolreza Zahiri conceived the study, collected the input data, developed the methodology, prepared the results, and supervised the research. Mohammad Reza Nikoo contributed to the development of the methodology, participated in the analysis and interpretation of the results, contributed to the conclusions, and critically revised the manuscript. Hamed Feiz Abady drafted the manuscript, prepared and edited the figures, organized and formatted the manuscript for submission, and contributed to manuscript revision. All authors read and approved the final manuscript.

9. Data Availability

The datasets analysed during the current study include reservoir water-level records provided by the Golestan Regional Water Authority and Sentinel-2 satellite imagery processed through

Google Earth Engine. The satellite imagery is publicly available through the Copernicus programme, whereas the reservoir water-level data are subject to data ownership restrictions and are therefore not publicly available. Processed data supporting the findings of this study are available from the corresponding author upon reasonable request and with permission from the Golestan Regional Water Authority, where applicable.

10. Acknowledgements

The authors used generative artificial intelligence tools solely to assist in the graphical refinement of the conceptual illustrations presented in Figures 3 and 4, as well as for limited language editing. All scientific content, methodologies, analyses, results, interpretations, and conclusions were developed, verified, and approved by the authors.

11. References

Adjovu, G.E., Stephen, H., James, D., & Ahmad, S. (2023). Overview of the application of remote sensing in effective monitoring of water quality parameters. *Remote Sensing*, *15*(7), 1938. https://doi.org/10.3390/rs15071938.

Alegría, A., Poloczanska, E., Loeschke, S., Mintenbeck, K., & Poertner, H. (2024). Towards an IPCC Atlas for comprehensive climate change risk assessments. Npj Climate Action, 3(1). https://doi.org/10.1038/s44168-024-00193-3.

Arrieta-Pastrana, A., Coronado-Hernández, O.E., & Fuertes-Miquel, V.S. (2024). Development of an explicit water level pool routing method in reservoirs. Water, 16. https://doi.org/10.3390/w16142042.

Avisse, N., Tilmant, A., Müller, M.F., & Zhang, H. (2017). Monitoring small reservoirs' storage with satellite remote sensing in inaccessible areas. *Hydrology and Earth System Sciences*, 21(12), 6445-6459. https://doi.org/10.5194/hess-21-6445-2017.

Boulange, J., Hanasaki, N., Yamazaki, D. & Pokhrel, Y. (2021). Role of dams in reducing global flood exposure under climate change. *Nat Commun*, 12, 417. https://doi.org/10.1038/s41467-020-20704-0.

Chagas, M.C., Falcão, A.P., & Oliveira, R.P.D. (2025). Using Sentinel imagery for mapping and monitoring small surface water bodies. Remote Sensing, 17(13), 2128. https://doi.org/10.3390/rs17132128.

Che, L., Li, S., & Liu, X. (2025). Improved surface water mapping using satellite remote sensing imagery based on optimization of the Otsu threshold and effective selection of remote-sensing water index. Journal of Hydrology, 654, 132771. https://doi.org/10.1016/j.jhydrol.2025.132771

Chen, C., Gao, X., Wu, M., Zhu, C., An, C., Li, D., & Liu, J. (2023). Optimizing the flood limit water level of reservoirs in sediment-laden rivers under changing water and sediment conditions: A case study of the Xiaolangdi Reservoir. *Water, 15*(20), 3552. https://doi.org/10.3390/w15203552.

649 Condeça, J., Nogueira, M., & Rodrigues, R. (2022). Reconstruction of reservoir storage dynamics using
650 Landsat and Sentinel imagery within Google Earth Engine. *Remote Sensing, 14*(17), 4302.
651 https://doi.org/10.3390/rs14174302.
652 Du, Y., Zhang, Y., Ling, F., Wang, Q., Li, W., & Li, X. (2016). Water bodies' mapping from Sentinel-2
653 imagery with modified normalized difference water index at 10-m spatial resolution produced by
654 sharpening the SWIR band. *Remote Sensing*, 8(4), 354. https://doi.org/10.3390/rs8040354.
655 Elfeki, A., Masoud, M., Basahi, J., & Zaidi, S. (2020). A unified approach for hydrological modeling of arid
656 catchments for flood hazards assessment: case study of Wadi Itwad, southwest of Saudi Arabia.
657 *Arabian Journal of Geosciences*, *13*(12), 490. https://doi.org/10.1007/s12517-020-05430-7.
658 Foteh, R., Garg, V., Nikam, B.R., Khadatare, M.Y., Aggarwal, S.P., & Kumar, A.S. (2018). Reservoir
659 sedimentation assessment through remote sensing and hydrological modelling. *Journal of the Indian*
660 *Society of Remote Sensing*, *46*(11), 1893-1905. https://doi.org/10.1007/s12524-018-0843-6.
661 Furnans, J., & Austin, B. (2008). Hydrographic survey methods for determining reservoir volume.
662 *Environmental Modelling & Software*, 23, 139-146. doi:10.1016/j.envsoft.2007.05.011.
663 Jaskuła, J., & Sojka, M. (2019). Analysis of degradation processes in reservoirs on the basis on
664 remote sensing data. Acta Scientiarum Polonorum. Formatio Circumiectus, *18*(2), 23-37.
665 https://doi.org/10.15576/asp.fc/2019.18.2.23.
666 Ji, L., Zhang, L., & Wylie, B. (2009). Analysis of dynamic thresholds for the normalized
667 difference water index. Photogrammetric engineering & remote sensing, 75(11), 1307-
668 1317. https://doi.org/10.14358/pers.75.11.1307.
669 Kaplan, G., & Avdan, U. (2017). Object-based water body extraction model using
670 Sentinel-2 satellite imagery. *European Journal of Remote Sensing*, 50(1), 137-
671 143. https://doi.org/10.1080/22797254.2017.1297540.
672 Khalifeh Soltanian, F., Abbasi, M., & Riyahi Bakhtyari, H.R. (2019). Flood monitoring using NDWI and
673 MNDWI spectral indices: A case study of Aghqala flood-2019, Golestan Province, Iran. *The*
674 *International Archives of the Photogrammetry, Remote Sensing and Spatial Information Sciences*, 42,
675 605-607. https://doi.org/10.5194/isprs-archives-xlii-4-w18-605-2019.
676 Kim, J.G., Kang, B., & Kim, S. (2022). Flood inflow estimation in an ungauged simple serial cascade of
677 reservoir system using Sentinel-2 multi-spectral imageries: A case study of Imjin River, South Korea.
678 *Remote Sensing*, 14(15), 3699. https://doi.org/10.3390/rs14153699.
679 Lai, Y.G., Huang, J., & Greimann, B.P. (2024). Hydraulic flushing of sediment in reservoirs: Best practices
680 of numerical modeling. *Fluids*, *9*(2), 38. https://doi.org/10.3390/fluids9020038.
681 Liu, C., Hu, R., Wang, Y., Lin, H., Zeng, H., Wu, D., & Shao, C. (2022). Monitoring water
682 level and volume changes of lakes and reservoirs in the Yellow River basin using ICESat-2

683 laser altimetry and Google Earth Engine. *Journal of Hydro-Environment Research*, 44, 53-
684 64. https://doi.org/10.1016/j.jher.2022.07.005.
685 Ma, Q., Xie, C., Duan, Z., Zhang, Y., Xiong, L., & Xu, C.-Y. (2025). Reconstruction of the reservoir water
686 level–storage volume relationship based on the capacity loss induced by sediment accumulation and
687 its impact on flood control operation. *Hydrology and Earth System Sciences, 29*, 6631–6646.
688 https://doi.org/10.5194/hess-29-6631-2025.
689 Mahato, P.S., & Ikbal, J. (2025). Shoreline Dynamics in the Sundarbans Delta (1975–2022): A Multi-
690 decadal Remote Sensing Assessment. *Asian Journal of Geological Research*, *8*(3), 587-603.
691 https://doi.org/10.9734/ajoger/2025/v8i3217.
692 Mahmood, M. R., Abrahem, B. I., Jumaah, H. J., Alalwan, H. A., & Mohammed, M. M. (2025). Drought
693 monitoring of large lakes in Iraq using remote sensing images and normalized difference water index
694 (NDWI). Results in Engineering, 25, 103854. https://doi.org/10.1016/j.rineng.2024.103854.
695 McFeeters, S.K. (1996). The use of the Normalized Difference Water Index (NDWI) in the
696 delineation of open water features. *International Journal of Remote Sensing*, 17(7):1425-
697 32. https://doi.org/10.1080/01431169608948714.
698 Nematollahi, B., Nikoo, M.R., Talebbeydokhti, N., Rakhshandehroo, R., Al-Raoush, R.I., and Chen, M.
699 2024. Reservoir release allocation and weir design MATLAB® toolbox. *Hydrological Sciences*
700 *Journal*, 68:15, 2141-2153, https://doi.org/10.1080/02626667.2023.2246956.
701 Nikoo, M.R., Zamani, M.G., Mohammad Zadeh, M., Al-Rawas, G., Al-Wardy, M., & Gandomi, A.H.
702 (2024). Mapping reservoir water quality from Sentinel-2 satellite data based on a new approach of
703 weighted averaging: Application of Bayesian maximum entropy. *Scientific Reports,* 14:16438.
704 https://doi.org/10.1038/s41598-024-66699-2.
705 Pogorelov, A.V., Doumit, J.A., & Laguta, A. (2024). Morphological evolution of the Krasnodar Reservoir
706 bed (2006–2021): Insights from geomorphometric analysis and benthic form transformations.
707 *International Journal in Information Technology in Governance, Education and Business, 7*(1).
708 https://doi.org/10.32664/ijitgeb.v7i1.172.
709 Ren, S., Gao, Y., Wang, W.-J., Zhou, Y., & Zhao, H. (2024). Estimating sediment trap efficiency of flood
710 events during flood season in the Three Gorges Reservoir. *Water Resources Research, 60*(4),
711 e2023WR036975. https://doi.org/10.1029/2023WR036975.
712 Safaripour, M., Monavari, M., Zare, M., Abedi, Z., & Gharagozlou, A. (2012). Flood risk assessment using
713 GIS (case study: Golestan province, Iran). Pol. J. Environ. Stud, 21(6), 1817-1824.
714 Schwatke, C., Dettmering, D., & Seitz, F. (2020). Volume variations of small inland water bodies from a
715 combination of satellite altimetry and optical imagery. Remote Sensing, 12(10), 1606.
716 https://doi.org/10.3390/rs12101606.

Schwatke, C., Dettmering, D., Scherer, D., & Seitz, F. (2021). Automated extraction of consistent time-variable water surfaces of lakes and reservoirs based on Landsat and Sentinel-2. Remote Sensing, 13(3), 447. https://doi.org/10.3390/rs13030447.

Singh, J., Singh, M.C., & Mathur, A. (2025). Assessment of reservoir capacity and sedimentation rate in Chohal Dam, Punjab, India, using multi-satellite data. *Water Supply*, *25*(5), 844-861. https://doi.org/10.2166/ws.2025.055.

Suresh, S., Hossain, F., Minocha, S., Das, P., Khan, S., Lee, H., & Oddo, P. (2024). Satellite-based tracking of reservoir operations for flood management during the 2018 extreme weather event in Kerala, India. *Remote Sensing of Environment*, 307, 114149. https://doi.org/10.1016/j.rse.2024.114149.

Verpoorter, C., Kutser, T., & Tranvik, L. (2012). Automated mapping of water bodies using Landsat multispectral data. *Limnology and Oceanography*: Methods, 10(12), 1037-1050. https://doi.org/10.4319/lom.2012.10.1037.

Xia, H., Zhao, J., Qin, Y., Yang, J., Cui, Y., Song, H., & Meng, Q. (2019). Changes in water surface area during 1989–2017 in the Huai River Basin using Landsat data and Google earth engine. *Remote Sensing*, 11(15), 1824. https://doi.org/10.3390/rs11151824.

Xia, X., Pan, J., & Pei, J. (2024). A new approach to estimate total nitrogen concentration in a seasonal lake based on multi-source data methodology. *Ecological Informatics*, *83*, 102807. https://doi.org/10.1016/j.ecoinf.2024.102807.

Xiaoyan, L.I.U., Yaoping, C.U.I., Zhifang, S.H.I., Yiming, F.U., Yadi, R.U.N., Mengdi, L.I., & Sujie, L.I.U. (2023). Monitoring of floods using multi-source remote sensing images on the GEE platform. *National Remote Sensing Bulletin*, 27(9), 2179-2190. https://doi.org/10.3724/sp.j.1047.2008.00102.

Xu H. (2006). Modification of normalised difference water index (NDWI) to enhance open water features in remotely sensed imagery. *International Journal of Remote Sensing*, 27(14), 3025-3033. https://doi.org/10.1080/01431160600589179.

Yao, F., Minear, J.T., Rajagopalan, B., Wang, C., Yang, K., & Livneh, B. (2023). Estimating reservoir sedimentation rates and storage capacity losses using high-resolution Sentinel-2 satellite and water level data. *Geophysical Research Letters*, *50*(16), e2023GL103524. https://doi.org/10.1029/2023gl103524.

Zhao, H., Yang, Z., Zhang, H., Meng, J., Jin, Q., & Ming, S. (2022). Emergency monitoring of a tailings pond leakage accident based on the GEE platform. *Sustainability*, *14*(14), 8558. https://doi.org/10.3390/su14148558.

Zhao, M., Liu, Y., Wang, Y., Chen Y., & Ding, W. (2022). Effectiveness assessment of reservoir projects for flash flood control, water supply and irrigation in Wangmo Basin, China. Science of the Total Environment, 851, Part 2, 157918. https://doi.org/10.1016/j.scitotenv.2022.157918.

751 Zhou, Y., Dong, J., Xiao, X., Xiao, T., Yang, Z., Zhao, G., & Qin, Y. (2017). Open surface water mapping
752 algorithms: A comparison of water-related spectral indices and sensors. Water, 9(4), 256.
753 https://doi.org/10.3390/w9040256.
754 Zhou, Y., Zhang, M., Li, Y., Wang, H., & Chen, X. (2024). Spatiotemporal evolution and influencing factors
755 of flood control storage sedimentation in the Three Gorges Reservoir, Changjiang River, China.
756 *CATENA, 243*, 108214. https://doi.org/10.1016/j.catena.2024.108214.